Am J Transl Res 2021;13(4):2077-2093
www.ajtr.org /ISSN:1943-8141/AJTR0113513

Original Article

Recombinant Chinese Hu191 measles virus exhibits a significant antitumor activity against nephroblastoma mediated by immunogenic form of apoptosis

Mengying Zhu[1*], Yilong Wang[2,3,4*], Chufan Qu[1], Rongxian Liu[1], Chudi Zhang[1], Jinhu Wang[2,4], Dongming Zhou[2,3], Weizhong Gu[2,3], Peichun Chen[5], Benqing Wu[5], Zhengyan Zhao[1,2,4]

[1]Zhejiang University School of Medicine, Hangzhou, Zhejiang, China; [2]Children's Hospital, Zhejiang University School of Medicine, Hangzhou 310052, Zhejiang, China; [3]Department of Neurology, Children's Hospital, Zhejiang University School of Medicine, Hangzhou 310052, Zhejiang, China; [4]Children's Hospital, Zhejiang University School of Medicine, National Clinical Research Center for Child Health, Hangzhou 310052, Zhejiang, China; [5]Maternal and Child Health Hospital of Guangming District, Shenzhen 518000, Guangdong, China. [*]Co-first authors.

Received April 28, 2020; Accepted February 2, 2021; Epub April 15, 2021; Published April 30, 2021

Abstract: In previous studies oncolytic measles viruses (MVs) have shown significant antitumor activity against various tumors. In our research recombinant MV-Hu191 (rMV-Hu191), established via reverse genetics technology and expressing enhanced green fluorescent protein (EGFP), was evaluated for its therapeutic effects and related mechanisms against nephroblastoma cell lines. We built three different constructs based on rMV-Hu191 to express EGFP effectively. Our experiments showed that rMV-Hu191 expressing EGFP could efficiently infect and replicate in nephroblastoma cell lines. Caspase-induced apoptosis exerted a significant impact on MV-induced cell death, which was accompanied by emission of cellular ATP and high-mobility group protein 1 (HMGB1) and by translocation of calreticulin (CRT). Intratumoral injection of rMV-Hu191-EGFP resulted in significant regression of tumors in a G401 xenograft model. Our results indicate that the MV-Hu191 strain, which is widely used in China, is an appropriate vector for expression of foreign genes and could serve as a potentially good candidate for nephroblastoma therapy mediated by induction of apoptosis-associated immunogenic cell death (ICD).

Keywords: Nephroblastoma, recombinant measles virus, reverse genetics, antitumor activity, apoptosis, immunogenic cell death

Introduction

Nephroblastoma, also known as Wilm's tumor, is the most common abdominal malignancy in children [1]. Although dramatic advances have been made during the past few decades in the treatment of nephroblastoma [2], nearly 12% of new cases are at risk of tumor relapse following frontline treatment [3, 4]. Patients with advanced stage and early relapse have a very poor prognosis, and their mortality rate remains high [5, 6]. On the other hand, patients who receive treatment, such as surgery, chemotherapy or radiotherapy, suffer from typically severe side effects [7]; therefore, new treatment strategies for nephroblastoma that are both safe and effective are strongly needed.

Oncolytic virotherapy began more than a century ago but has emerged recently as a promising approach for treating cancer. Oncolytic viruses (OVs) can mediate antitumoral responses by direct lytic effects on tumor cells and by induction of systemic antitumoral immune responses [8]. During the past two decades, reverse genetic techniques have enabled a variety of OVs to display great potential for treatment of multiple tumor types including lung and hepatocellular carcinoma, colorectal cancer, melanoma, breast cancer, neuroglioma, and ovarian cancer [9-15]. Among the numerous OVs currently used for antitumoral therapy, attenuated strains of measles virus (MV) have demonstrated a valid oncolytic activity against a variety of human tumor types [16, 17]. Thus,

MV is an attractive platform for use as a safe and effective oncolytic vector [18].

MV (family *Paramyxoviridae*; order *Mononegavirales*) is an enveloped virus with a non-segmented, negative-sense RNA genome [19]. Formation of multinuclear cell aggregates (syncytia) is the typical cytopathic effect (CPE) of MV, as infected cells fuse with the surrounding cells [20]. In contrast, attenuated MV vaccine strains infect cells predominantly via the complement regulator CD46 (also known as membrane cofactor protein; MCP), which is commonly overexpressed on the surface of tumor cells [16, 21, 22]. Poliovirus receptor-like protein 4 (nectin-4), which has also been identified as overexpressed on many malignant cell types, has been identified as the epithelial cell receptor for MV [23, 24]. The Edmonston live-attenuated vaccine strain (MV-Edm) selectively infects and kills cancer cells that overexpress CD46 and nectin-4 [25-27]. Several advancements have been made in the design and development of MV-Edm derivatives, and exogenous genes have been inserted and expressed from different loci of its genome [28-31]. In reported clinical trials both unmodified attenuated MV-Edm strain and engineered oncolytic MV strains expressing human carcinoembryonic antigen (CEA) and human thyroidal iodide symporter (NIS) were well tolerated without dose-limiting toxicity. A phase I clinical trial of MV strains expressing the human thyroidal iodide symporter (NIS) is being conducted to treat Medulloblastoma or atypical rhabdoid tumor in children and young adults [32].

The Hu191 strain (MV-Hu191) was developed in the early 1960s as a live-attenuated vaccine. This strain is widely used for immunization in all provinces of China and has been administered to millions of individuals in China with an excellent safety record [33]. Because MV-Hu191 is an authorized vaccine in China, it is an optimal candidate to consider as a cancer therapy that exploits the oncolytic activity of MVs [34]. We found that rMV-Hu191 with enhanced green fluorescent protein (EGFP) inserted in the noncoding region between the H and L genes had remarkable antitumor activity in nephroblastoma cell lines *in vivo* and *in vitro*. MV induced cell lysis by direct cell killing through formation of a syncytium [35]. Our results showed that apoptosis played an important role for MV-induced cell death and for apoptotic nephroblastoma cell death accompanied by immunogenic cell death. The latter was characterized by the cell-surface exposure of calreticulin (CRT) and by the emission of ATP and high-mobility group box 1 (HMGB1).

Material and methods

Cells and virus

Vero cells (African green monkey, ATCC-CCL-81) and BHK-SR19-T7 cells [36] (kindly offered by Apath, LLC, Brooklyn, NY) were grown in Dulbecco's modified Eagle's medium (DMEM; Life Technologies) supplemented with 10% fetal bovine serum (FBS). G401 and SK-NEP-1 cells were purchased from the Type Culture Collection of the Chinese Academy of Sciences in Shanghai, China and were maintained in McCoy's 5A medium (Gibco/Life Technologies) supplemented with 10% heat-inactivated FBS (Gibco/Life Technologies), 100 U/ml penicillin, and 100 μg/ml streptomycin (Gibco/Life Technologies). Cell lines were incubated at 37°C in a humidified atmosphere containing 5% CO_2. rMV-Hu191 recovered from a previous study [34] was maintained at -80°C and was passed in Vero cells in our lab.

Construction and virus titration of rMVs expressing EGFP

rMVs containing the EGFP gene inserted in the N, P, or H genes were constructed. Briefly, two DNA fragments containing the EGFP gene along with the gene start and gene end sequence of MV-Hu191 were obtained by gene synthesis (Huada, Shanghai, China), and then were inserted into the plasmids pEASY-N, pEASY-P, or pEASY-H from our previous work [34, 37, 38]. These insertions produced pEASY-MV-N-EGFP, pEASY-MV-P-EGFP and pEASY-MV-H-EGFP (**Figure 1A1-C1**). Plasmids pYES-MV-N-EGFP (+), pYES-MV-P-EGFP (+) and pYES-MV-H-EGFP (+) were assembled from ten fragments using the GeneArt™ High-Order Genetic Assembly System on the basis of the manufacturer's manual (**Figure 1A2-C2**). Plaque assays in Vero cells were used to quantify infectious titers of rMV-Hu191.

Assessment of fluorescence

Five thousand Vero cells were plated in each well of 96-well plates; then, after 24 h the cells were infected with rMV-Hu191-N-EGFP, rMV-Hu191-P-EGFP or rMV-Hu191-H-EGFP at a multiplicity of infection (MOI) of 0.1. After a one-hour incubation, the original medium for absorption was replaced by DMEM containing 2%

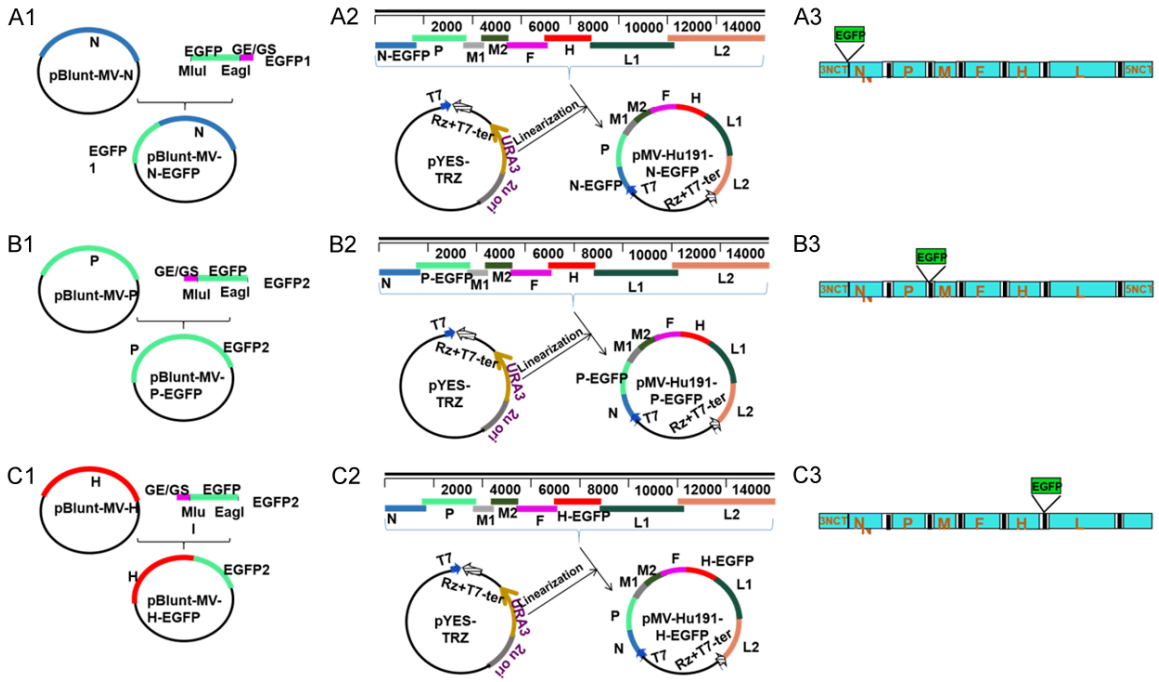

Figure 1. Construction of full-length cDNA clones of rMVs expressing EGFP. EGFP (EGFP1, EGFP2) gene with gene start and gene end of MV was inserted into pEASY-MV-N, pEASY-MV-P and pEASY-MV-H plasmids using a seamless cloning strategy to generate pEASY-MV-N-EGFP, pEASY-MV-P-EGFP and pEASY-MV-H-EGFP (A1, B1, C1). Eight overlapping fragments including the full-length MV genome and EGFP gene were assembled into p107109-MV (+), generating full-length cDNA plasmid pYES-MV-Hu191-N-EGFP, pYES-MV-Hu191-P-EGFP, pYES-MV-Hu191-H-EGFP (A2, B2, C2). Schematic representation of insertion of EGFP within different loci of the MV-Hu191 genome (A3, B3, C3).

FBS. At 24, 48, 72 or 96 h post-infection (hpi), the fluorescence value was measured using a SYNERGY H1 microplate reader (excitation/emission: 480/520 nm) (BioTek, USA).

Assessment of CPE in vitro

5×10^5 per well of nephroblastoma cell lines were plated into 6-well plates and were infected with rMV-Hu191-H-EGFP at a MOI of 0.1. Fusion was measured by recording green fluorescence syncytia. 5×10^5 per well of G401 or SK-NEP-1 cells were plated into 6-well plates and were infected 24 h later with rMV-Hu191-H-EGFP at a MOI of 0.1 or 1. At 24, 36 and 48 hpi, the cells infected with rMV-Hu191 were fixed with 4% paraformaldehyde (PFA) in PBS for 20 minutes at room temperature (RT). Finally, cells were stained with 0.1% crystal violet solubilized in 100% ethanol.

Viral replication kinetics in nephroblastoma cell lines

1×10^5 per well of G401 or SK-NEP-1 cells were plated into 24-well plates and were infected after 24 h with rMV-Hu191 viruses at a MOI of 0.1 or 1. At different time points post-infection, the cells were harvested by three freeze-thaw cycles, and supernatants were collected after centrifugation at 3,000×g in a 5810R centrifuge (Eppendorf) for 15 minutes. Infectious titers were determined by plaque assay in Vero cells.

Cell viability assay

1×10^4 per well of G401 and SK-NEP-1 cells were plated into 96-well plates; then, 24 h after seeding, the cells were infected with rMV at different MOIs (0.01, 0.1, 1 and 10). At 24, 48, 72, and 96 hpi, cell viability was evaluated using a Cell Counting Kit-8 (Dojindo Molecular Technologies). Spectrophotometric absorbance was measured at a wavelength of 450 nm using a microplate reader (Thermo Fisher), and the number of viable cells per well was predicted from its absorbance using an external calibration (standard curve).

Detection of CD46 and nectin-4 expression by G401 or SK-NEP-1

5×10^5 cells were first incubated with primary antibody diluted in PBS-milk in darkness for 30 minutes at RT and washed. Cells were incubat-

ed with secondary antibodies as needed and were analyzed by flow cytometry (BD Biosciences). The antibodies used in the studies were as follows: PE mouse anti-human CD46 antibody (RD, AF2659), anti-human nectin-4 antibody (BD 564252), and rabbit anti-goat IgG (H+L) secondary antibody labeled with Alexa Fluor 594 (Invitrogen, A27016).

Annexin V staining and apoptosis analysis

G401 and SK-NEP-1 cells were inoculated with rMV-Hu191-H-EGFP at a MOI of 0.1. After 48 hpi, the cells were collected for apoptosis analysis by FITC Annexin V Apoptosis Detection kit (BD). The dead cells were stained with both FITC Annexin V and PI and were analyzed by flow cytometry (Beckman).

DNA fragmentation assay

DNA was acquired by the standard phenol/chloroform extraction method, was analyzed by gel electrophoresis, and was visualized by ultraviolet light after DNA dye staining.

Western blot analysis

Expression of caspase-3, cleaved caspase-3, poly ADP-ribose polymerase (PARP) and cleaved PARP was studied in nephroblastoma cells and tumor tissues. After lysing cells with lysis buffer (RIPA) and incubating on ice for 15 minutes, protein was harvested by centrifugation at 12000×g for 15 min at 4°C. The BCA method was used to identify the protein concentration, and soluble protein added to 5× loading buffer was incubated for 10 min at 100°C. Samples were separated by 12% SDS-polyacrylamide gel electrophoresis and were transferred to activated PVDF membranes. The membranes were then blocked with 5% skim milk for 2 h at RT. Primary antibodies (rabbit anti-β-actin antibody [CST 4970S], rabbit anti-PARP antibody [CST 9542S] and rabbit anti-caspase-3 antibody [CST 9662S]) were mixed for 12 h at 4°C and then were incubated with a second antibody (goat anti-rabbit IgG [CST 7074s]) for 1 h at RT. Antigen-antibody complexes were visualized using an imaging system (SYNGENE G: BOX Chemi XRQ).

Examination of DAMPs

G401 and SK-NEP-1 cells were infected with rMV-Hu191-EGFP (MOI=0.5) for 48 h. We harvested the cells, stained them with anti-CRT antibody (Abcam) according to the protocol, and then measured surface CRT expression by flow cytometry. The amount of ATP in the cell culture media was evaluated with an ATP Assay Kit (Beyotime). HMGB1 in the cell culture media was quantified using an HMGB1 ELISA Kit (IBL International).

Assessment of oncolytic activity in vivo

All animal procedures conformed to the Guide for the Care and Use of Laboratory Animals and were approved by the Zhejiang University Medical Laboratory Animal Care and Use Committee. G401 cells (1×10^7) were implanted subcutaneously into the right flanks of nude mice. When the average tumor diameter reached ~100 mm^3, 8 mice were intratumorally administered 1×10^7 PFU of rMV-Hu191-H-EGFP (n=4) or Opti-MEM (n=4) every other day for 10 days. Mice were euthanized 4 days after the first inoculation, and their tumor samples were collected. To estimate effects of rMV-Hu191-H-EGFP on tumor growth, 28 mice were randomly divided into four groups (n=7 per group), receiving intratumoral injections of rMV-Hu191-H-EGFP (1×10^5, 1×10^6, or 1×10^7 PFU in a volume of 100 μl) or Opti-MEM (Life Technologies). Tumor volumes were measured twice weekly and were calculated as follows: tumor volume (mm^3) = length × $width^2$ × ½. All mice were euthanized at 29 days after the first viral infection. Some individual mice also were euthanized if tumor diameter reached 1 cm or if the individual had lost 20% of its body weight. After euthanasia, all tumors were collected and weighed.

Histology staining

The TUNEL assay was conducted to evaluate apoptotic cell death in tumor tissues according to the manufacturer's instructions. All tumor tissues were fixed in 4% PFA, embedded in paraffin, were cut into thin sections, and were stained by hematoxylin and eosin.

Statistical analysis

Tests of treatment effects of univariate outcomes were conducted using ANOVA with post-hoc multiple comparisons as implemented in the Prism statistical analysis software (version

8.0). Tests of treatment effects on multivariate outcomes, which were observed as a consequence of repeated measurements of an experimental unit, were conducted by fitting a linear model (LM) of multivariate normal responses. The model included parameters for the effects of treatment, time and treatment-time interactions and for an unstructured covariance matrix of responses. Tests of treatment effects on cell viability were conducted by fitting a generalized linear model (GLM) to the counts of viable cells observed after infection with rMV. The LM and the GLM were fit using the R software program (version 4.0). *P*-values <0.05 were considered statistically significant. *P*-values <0.01 were considered highly statistically significant.

Results

Generation and characterization of rMVs expressing EGFP

In order to generate a tool for easy observation, exogenous gene expressing EGFP was successfully inserted into the MV-Hu191 genome at three different positions (**Figure 1**). rMVs expressing EGFP (rMV-Hu191-N-EGFP, rMV-Hu191-P-EGFP and rMV-Hu191-H-EGFP) were successfully rescued. rMV-Hu191-H-EGFP induced cell fusion to a greater extent compared to the other two viruses after 36 h inoculation in Vero cells (**Figure 2A**). Subsequently, stability of EGFP expression was confirmed after 12 passages in Vero cells by immunofluorescence examination. The peak fluorescence intensity of rMV-Hu191-N-EGFP was clearly lower than rMV-Hu191-P-EGFP and rMV-Hu191-H-EGFP (**Figure 2B**). We then compared the CPE of the three EGFP mutants with that of the parental virus (rMV-Hu191) at a MOI of 0.1 in Vero cells. At 72 hpi, the CPE induced by rMV-Hu191-N-EGFP and by rMV-Hu191-P-EGFP was much weaker than the parental rMV-Hu191, whereas the CPE induced by rMV-Hu191-H-EGFP was similar to the parental rMV-Hu191 (**Figure 2C**). These results suggested that insertion of EGFP between the MV H and L genes hardly impaired CPE induction, although the fluorescence expression of rMV-Hu191-N-EGFP and rMV-Hu191-P-EGFP was much higher. Thus, rMV-Hu191-H-EGFP was an appropriate candidate for further study of the oncolytic effects of MV-Hu191.

rMV-Hu191 infected and caused significant CPE in nephroblastoma cell lines, exerting obvious antitumor effects in vitro

Previous research demonstrated that MV strains could generate a robust oncolytic activity against a wide range of cancer types. rMV-Hu191-H-EGFP infected G401 or SK-NEP-1 at a MOI of 0.1 or 1, and green fluorescence syncytia were formed. The total number of syncytia formed and their size, cellular complexity and fluorescence density varied significantly in relation with different MOI of virus (**Figure 3A**). Because CD46 and nectin-4 are the main receptors of MV, we evaluated their expression level on nephroblastoma cell lines (G401 and SK-NEP-1). High levels of CD46 were expressed in the human nephroblastoma cells (97.9% and 99.2% of G401 cells and SK-NEP-1 cells, respectively). Levels of nectin-4 in the human nephroblastoma cell lines were comparatively low (9.55% and 9.99% of G401 cells and SK-NEP-1 cells, respectively) (**Figure 3B**).

rMV-Hu191-H-EGFP, as an appropriate candidate for this study, infected nephroblastoma cell lines at a MOI of 0.1 and 1. Infected nephroblastoma cell lines exhibited a dramatic CPE compared to uninfected cells in a MOI-dependent manner at 24, 36 and 48 hpi (**Figure 3C**).

To investigate rMV-Hu191 replication efficiency, G401 and SK-NEP-1 cells were inoculated with rMV-Hu191 at MOI of 0.1 and 1, and virus titers were determined using plaque assay. As demonstrated in **Figure 3D**, rMV-Hu191 could replicate well in nephroblastoma cell lines and grew to a high titer.

We further evaluated the MOI-dependent decrease of cell viability by performing a CCK8 assay at 24, 48, 72 and 96 hpi. This test showed that rMV-Hu191 significantly reduced proliferation of G401 and SK-NEP-1 cells from 72-96 hpi at a MOI of 1 and 10 ($P<0.001$; **Figure 3E**).

Caspase-induced apoptosis plays a significant role in rMV-Hu191-H-EGFP-induced cell death

Several studies have shown that MV infection can result in apoptosis [39-41]. We hypothesized that rMV-Hu191-H-EGFP would induce

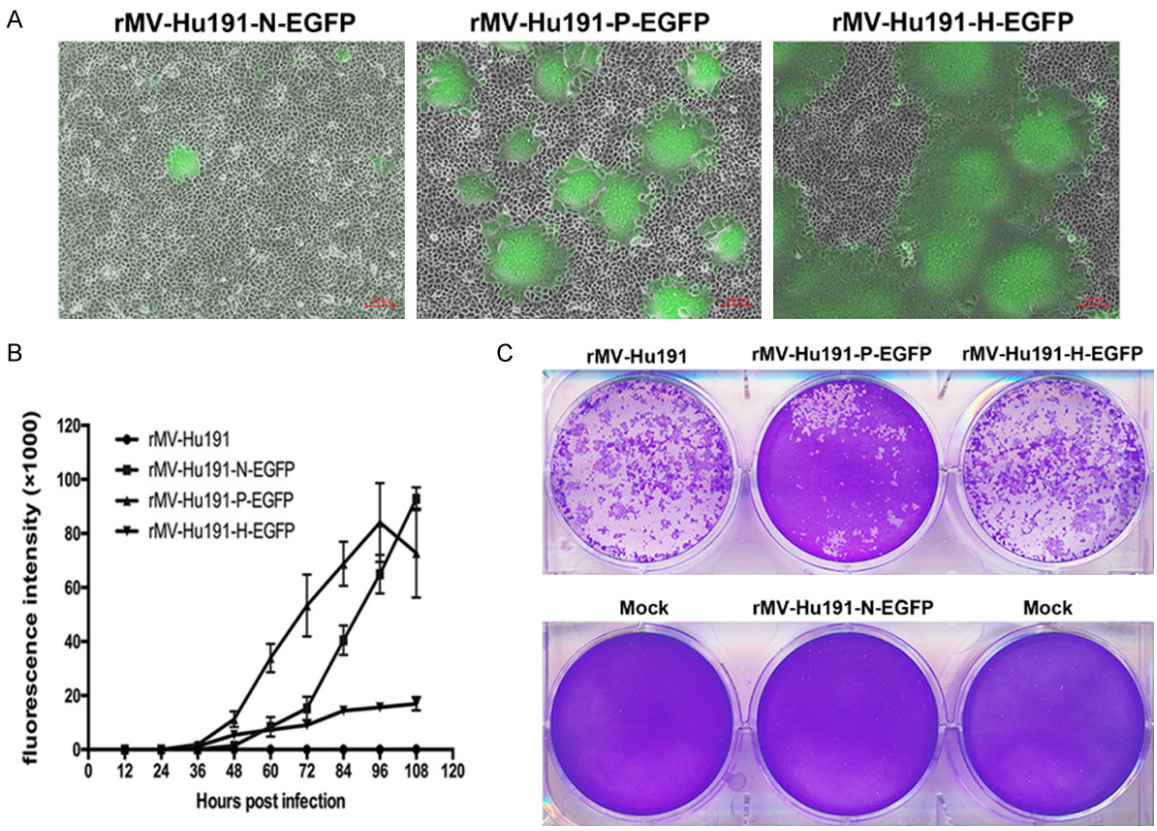

Figure 2. Verification EGFP expression of recombinant MV-Hu191-EGFP. A. rMV-Hu191-N-EGFP, rMV-Hu191-P-EGFP and rMV-Hu191-H-EGFP were passaged 10 times in Vero cells; confluent Vero cultures were inoculated with rMV-Hu191-N-EGFP (P10), rMV-Hu191-P-EGFP (P10) and rMV-Hu191-H-EGFP (P10) at MOI of 0.01, and syncytia were observed by fluorescence microscopy for EGFP at 36 hpi. Scale bars, 100 μm. B. Vero cells in 96-well plates were inoculated with each rMV at MOI of 0.01. Total fluorescence was detected by a SYNETGY H1 microplate reader (excitation/emission: 480/520 nm) (BioTek, USA) at 12, 24, 36, 48, 60, 72, 84, 96 and 108 hpi. Representative data from three independent experiments is shown. C. Vero cells were inoculated with each rMV at a MOI of 0.1. Cultures were stained with crystal violet at 72 hpi.

apoptotic death in nephroblastoma cell lines as well. G401 and SK-NEP-1 cells were infected with rMV-Hu191-H-EGFP at MOI of 0.1. After 72 hpi, infected cells were collected for fluorescence-activated cell sorting (FACS) analysis after staining with Annexin V and propidium iodide to detect apoptosis. Apoptosis was induced followed infection with rMV-Hu191-H-EGFP at MOI of 0.1. There was no obvious apoptosis in uninfected cells (**Figure 4A**). Total DNA fragmentation assay revealed a ladder-like pattern of DNA fragments consistent with internucleosomal fragmentation in apoptotic death (**Figure 4B**). Subsequently, apoptosis pathways were identified by Western blot, detecting expression of the key proteins caspase-3 and PARP, a substrate for caspase activity. From 24-60 hpi, expression levels of cleaved PARP, cleaved caspase-3 increased from 36-60 hpi (**Figure 4C**). Apoptosis in infected G401 and SK-NEP-1 cells was apparently inhibited following incubation with caspase inhibitor Z-VAD-FMK (Z-VAD) (**Figure 4D**, **4E**).

rMV-Hu191-H-EGFP-induced apoptosis was characterized with emission of DAMPs

It has been reported that syncytia formed by viral fusogenic membrane glycoproteins can lead to ICD [35, 42, 43]. According to current research, the characteristics of ICD are mainly mediated by DAMPs, such as translocated CRT, passively released HMGB1 and secreted ATP, which are required for ICD and leads to activation of potent anticancer immunity [44-46]. To detect surface CRT expression, two nephroblastoma cell lines were inoculated with rMV-Hu191-H-EGFP at MOI of 0.5. After 48 hpi, the cells were collected for detecting CRT expres-

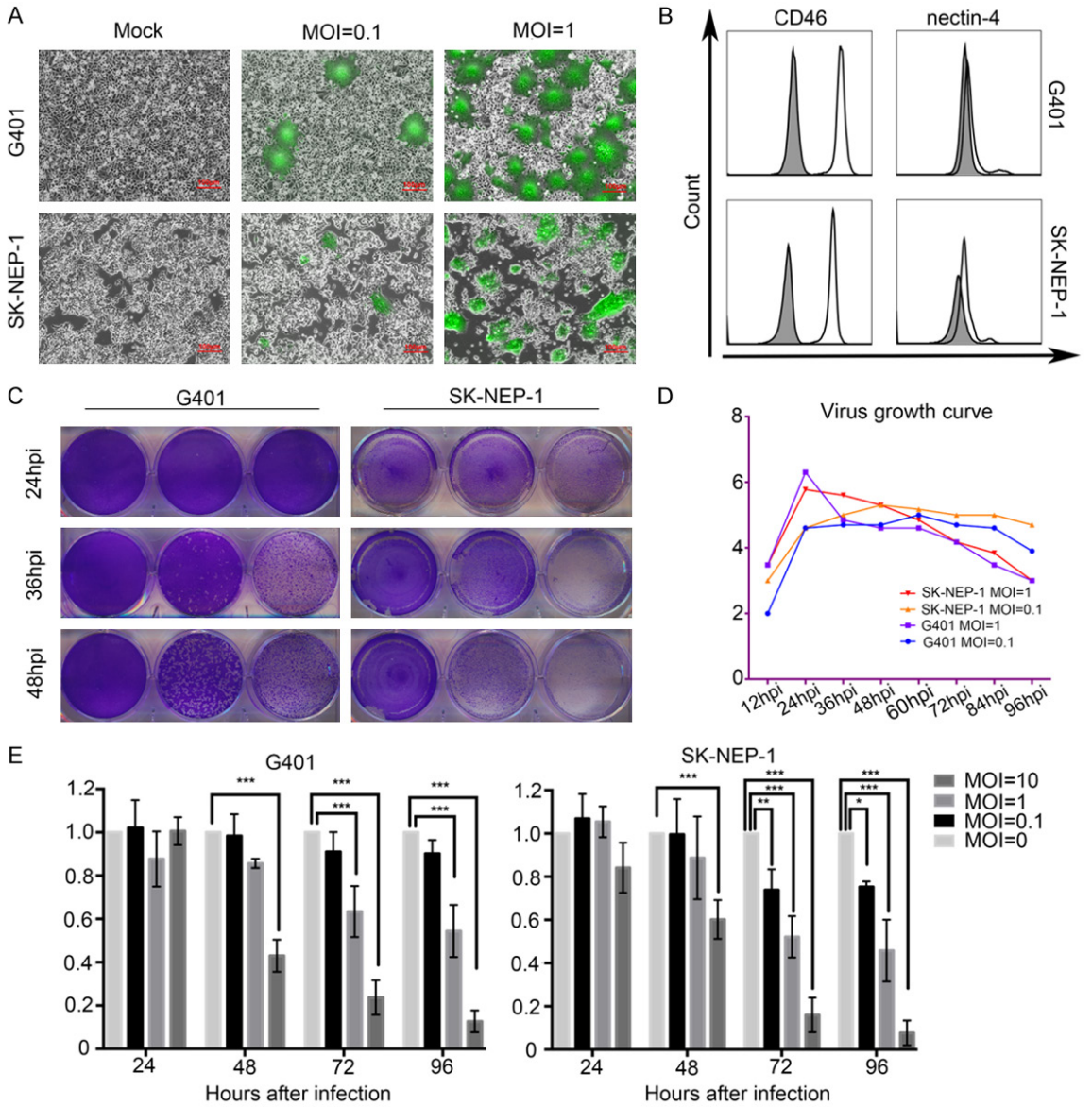

Figure 3. Expression of MV receptors on human nephroblastoma cells, cytopathic effect, viral growth and killing ability of rMV-Hu191-H-EGFP in nephroblastoma cell lines. A. G401 or SK-NEP-1 exhibited fluorescence at 24 hpi with MV-infection of different MOI. B. 10^6 cells were labeled with primary and secondary antibodies, and flow cytometry was performed to evaluate the expression level of CD46 and nectin-4 receptors. The grey histogram represents the isolated IgG control for each cell line. C. Confluent G401 and SK-NEP-1 cells were infected with rMV-Hu191-H-EGFP. Cytopathic effects were determined in nephroblastoma cell lines by staining with crystal violet every 12 h. D. G401 and SK-NEP-1 cells in plates were infected with rMV-Hu191 at a MOI of 0.1 or 1, and supernatants and cells were collected after three freeze-thaw cycles. Viral titer was tested by plaque assay in Vero cells. Each data point represents Log virus titer at the different time points. E. Viability of G401 and SK-NEP-1 cell lines were detected by CCK-8 assay at 24, 48, 72 and 96 hpi. rMV-Hu191-H-EGFP effectively suppressed tumor cell proliferation. *=P<0.05; **=P<0.01; ***=P<0.001.

sion by flow cytometry. The surface CRT expression increased in infected G401 and SK-NEP-1 cells more than in uninfected control groups (**Figure 5A**). G401 and SK-NEP-1 cells were inoculated with rMV-Hu191-H-EGFP at a MOI of 0.1 or 1. The amount of ATP and HMGB1 in the supernatants then were determined at various time points. There were low levels of extracellular ATP after 12 h infection in both cell lines, but the amount of extracellular ATP released in G401 and SK-NEP-1 cells rose rapidly, reaching a peak at 24 hpi more quickly in cells infected

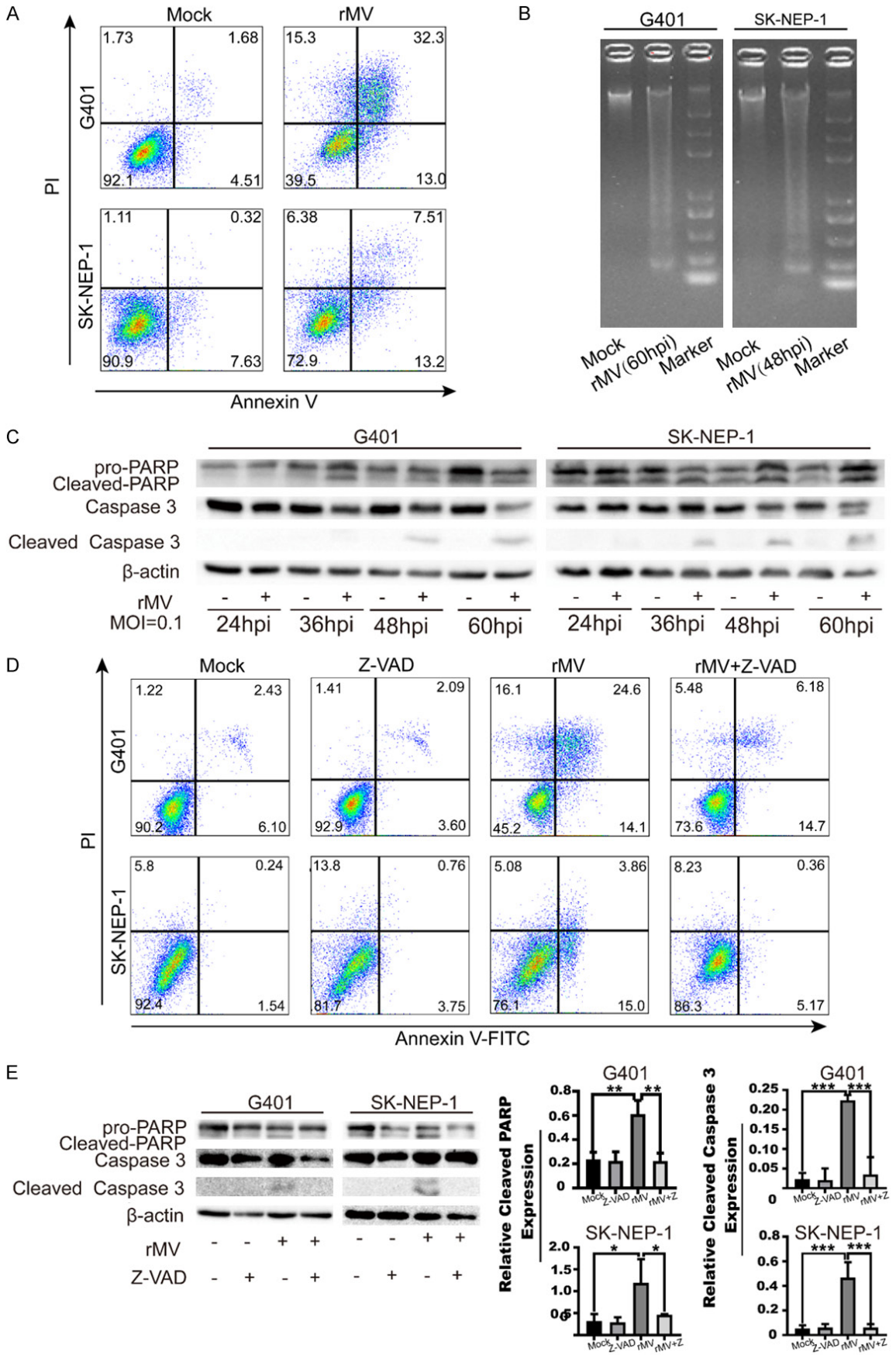
A
Mock
rMV
G401
SK-NEP-1
PI
Annexin V
1.73
1.68
92.1
4.51
15.3
32.3
39.5
13.0
1.11
0.32
90.9
7.63
6.38
7.51
72.9
13.2
B
G401
SK-NEP-1
Mock
rMV(60hpi)
Marker
Mock
rMV(48hpi)
Marker
C
G401
SK-NEP-1
pro-PARP
Cleaved-PARP
Caspase 3
Cleaved Caspase 3
β-actin
rMV
MOI=0.1
24hpi
36hpi
48hpi
60hpi
D
Mock
Z-VAD
rMV
rMV+Z-VAD
G401
SK-NEP-1
PI
Annexin V-FITC
1.22
2.43
90.2
6.10
1.41
2.09
92.9
3.60
16.1
24.6
45.2
14.1
5.48
6.18
73.6
14.7
5.8
0.24
92.4
1.54
13.8
0.76
81.7
3.75
5.08
3.86
76.1
15.0
8.23
0.36
86.3
5.17
E
G401
SK-NEP-1
pro-PARP
Cleaved-PARP
Caspase 3
Cleaved Caspase 3
β-actin
rMV
Z-VAD
Relative Cleaved PARP Expression
Relative Cleaved Caspase 3 Expression
Mock
Z-VAD
rMV
rMV+Z

Figure 4. rMV-Hu191-H-EGFP infection induces caspase-induced apoptosis *in vitro*. A. G401 and SK-NEP-1 cells were infected with rMV-Hu191-H-EGFP at a MOI of 0.1 and double-stained with Annexin V and propidium iodide (PI) flowed analysis by flow cytometry. The percentage of apoptotic cells (Annexin V+/PI- and Annexin V+/PI+) increased evidently after virus infection. Data shown are representative of three independent experiments. B. G401 and SK-NEP-1 cells were inoculated with rMV-Hu191-H-EGFP at a MOI of 0.5; DNA fragments were extracted and detected by agarose gel electrophoresis in infected tumor cells. C. G401 and SK-NEP-1 nephroblastoma cancer cells were infected with rMV-Hu191-H-EGFP at a MOI of 0.1 for 12, 24, 36, and 48 h. Cell lysates were harvested for Western blot to evaluate the levels of cleaved-PARP and cleaved-caspase-3. D. Both cells were infected with rMV-Hu191-H-EGFP at a MOI of 0.1 or 1. Western blot was performed to exam the levels of cleaved-PARP and cleaved-caspase-3 at 36 hpi. E. G401 and SK-NEP-1 cells were inoculated with rMV-Hu191-H-EGFP at an MOI of 0.1 in the presence of Z-VAD-FMK (Z-VAD) (Apexbio), and levels of cleaved-PARP and cleaved-caspase-3 were assessed by Western blot of cell lysates. Ratio of apoptotic cells after co-treated with Z-VAD and rMV-Hu191-H-EGFP decreased.

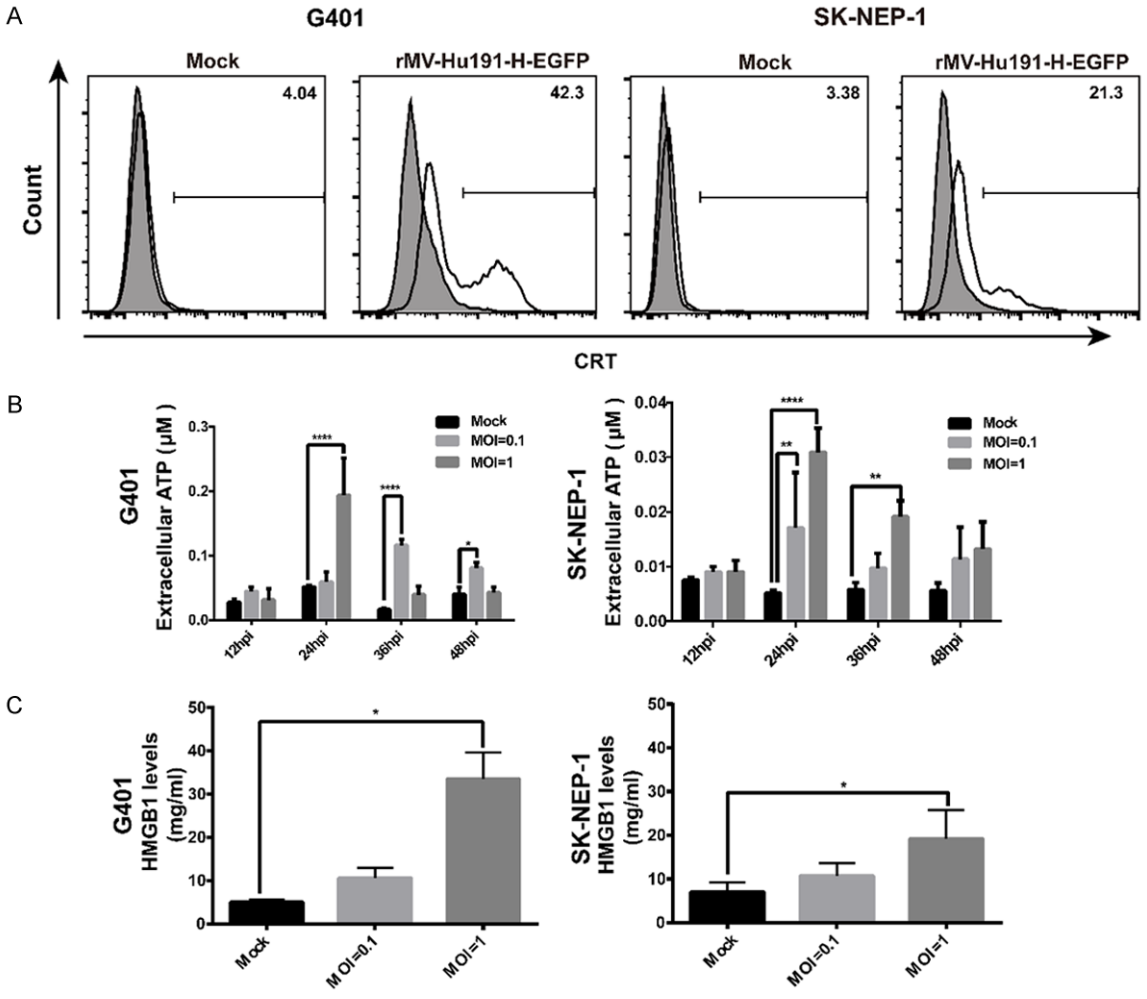

Figure 5. rMV-Hu191-H-EGFP induced immunogenic cell death (ICD) in Nephroblastoma cells. A. CRT exposure on G401 and SK-NEP-1 cells surface was analyzed at 48 h after rMV-Hu191-H-EGFP infection (MOI=0.5) by flow cytometric analysis. B. G401 and SK-NEP-1 cells were infected with rMV-Hu191-H-EGFP at a MOI=0.1, and supernatants were collected after 12, 24, 36 and 48 h incubation. The amounts of ATP in the supernatants were detected by an ATP Assay Kit. C. G401 and SK-NEP-1 cells were infected with rMV-Hu191-H-EGFP at a MOI of 0.1 for 36 h, supernatants were harvested, and HMGB1 levels in the supernatants were evaluated using an HMGB1 ELISA Kit. Time-course and multigroup analyses were carried out using analysis of variance (ANOVA). Data are reported as mean ± SD. *=P<0.05; **=P<0.01; ***=P<0.001; ****=P<0.0001.

at MOI of 1 than at MOI of 0.1 (**Figure 5B**). The levels of HMGB1 were low in each group of G401 and SK-NEP-1 cells, but markedly increased after 36 h inoculation at MOI of 1 (**Figure 5C**), with a significant difference (P< 0.001) between the groups.

Pharmacological inhibition of apoptosis influenced MV-induced cell death

To evaluate the importance of apoptosis in rMV-induced syncytial death, we incubated the rMV-Hu191-H-EGFP-infected G401 and SK-NEP-1 cells with the broad-spectrum caspase inhibitor Z-VAD. This inhibitor did not have a significant impact on the MV-induced syncytium formation, but the inhibitor prolonged the survival of MV-induced syncytia and inhibited MV-induced apoptosis in G401 and SK-NEP-1 cells (**Figure 6A**). **Figure 6B** and **6C** show that extracellular ATP concentrations and the expression level of the cell surface CRT in cell supernatants dropped evidently in groups upon MV infection along with Z-VAD compared to groups treated with virus alone.

rMV-Hu191-H-EGFP replicated efficiently and suppressed tumor growth in a G401 xenograft tumor model

To evaluate the antitumoral effects of rMV-Hu191-H-EGFP *in vivo*, G401 cells (5×10^6 cells/mouse) were implanted in the right flanks of nude mice, then mice were treated with intratumoral injections of PBS or rMV-Hu191-H-EGFP every other day for 10 days. Tumor mass was measured after euthanasia at 29 dpi, revealing that treatment with rMV-Hu191-H-EGFP had significantly inhibited tumor growth compared with the uninjected controls. We found that the MV-induced antitumor effect was MOI-dependent, as injection of 1×10^7 PFU of rMV-Hu191-H-EGFP resulted in elimination of tumors in all mice (**Figure 7A-D**). The difference in tumor volumes and masses was statistically significant ($P<0.001$) between mock and rMV-Hu191-H-EGFP treatment (**Figure 7A**, **7D**).

To observe viral replication in the tumor, four mice inoculated with 1×10^7 PFU rMV-Hu191-H-EGFP or PBS were euthanized at 15 dpi. EGFP could be detected in samples from infected tumors by fluorescence microscopy (**Figure 8A**), and N protein was detected by Western blot (**Figure 8B**). To investigate the role of caspase-3-mediated apoptosis on tumor death induced by rMV-Hu191-H-EGFP *in vivo*, expression of caspase-3 was detected by Western blot, showing an increase in the rMV-infected tumor samples (**Figure 8B**). To analyze the pathological changes of virus-infected tumor tissues, hematoxylin-eosin staining was performed on tumor tissues treated with rMV-Hu191-H-EGFP, revealing large necrotic areas and apoptotic cells (**Figure 8C**). To confirm the mechanism of cell death, we administrated a TUNEL assay on the paraffinized sections of tumor tissues from the G401 xenografts. TUNEL-positive cells were detected in the rMV-Hu191-H-EGFP infected tumors, whereas almost no TUNEL-positive cells were found in the mock-injected G401 xenograft tumors (**Figure 8C**).

Discussion

Although current therapeutic strategies for nephroblastoma are effective, the death rate remains high in patients with advanced stages and early relapse. Development of novel treatment regimens is of increasing urgency for these patients [4]. Oncolytic virotherapy is an emerging new strategy for tumor therapy that uses replication-competent viruses to destroy cancers [47]. Four viruses including vaccinia virus, herpes simplex virus-1, reovirus and Seneca Valley virus have been admitted into pediatric clinical trials [48].

MV represents a new generation of safe and effective oncolytic viruses [32], that have great potential for treatment of cancers. MV-Edm is widely and frequently used in oncolytic virotherapy [17], and vaccine derivatives have significant antitumor activity and thus important advantages as virotherapy agents. In reported clinical trials, both unmodified attenuated MV-Edm strain and engineered oncolytic MV-Edm strains were well tolerated without dose-limiting toxicity in studies of non-small cell lung cancer, ovarian cancer, malignant peripheral nerve sheath tumor medulloblastoma or atypical rhabdoid tumor in children and young adults. The most common adverse effects were fatigue and fever [32, 49-55]. With respect to regulatory issues, the lesser studied MV-Hu191 is a more suitable cancer virotherapy candidate in China.

To our knowledge, this is the first report to utilize MV-Hu191 as a treatment for nephroblastoma. As for MV-Edm, previous studies revealed that CD46 was the major receptor used to infect multiple cancer cell lines [25, 26, 56]. In our research, similar to what has been reported in the literature, susceptibility of nephroblastoma cell lines to rMV-Hu191 was associated with overexpression of the MV cell recep-

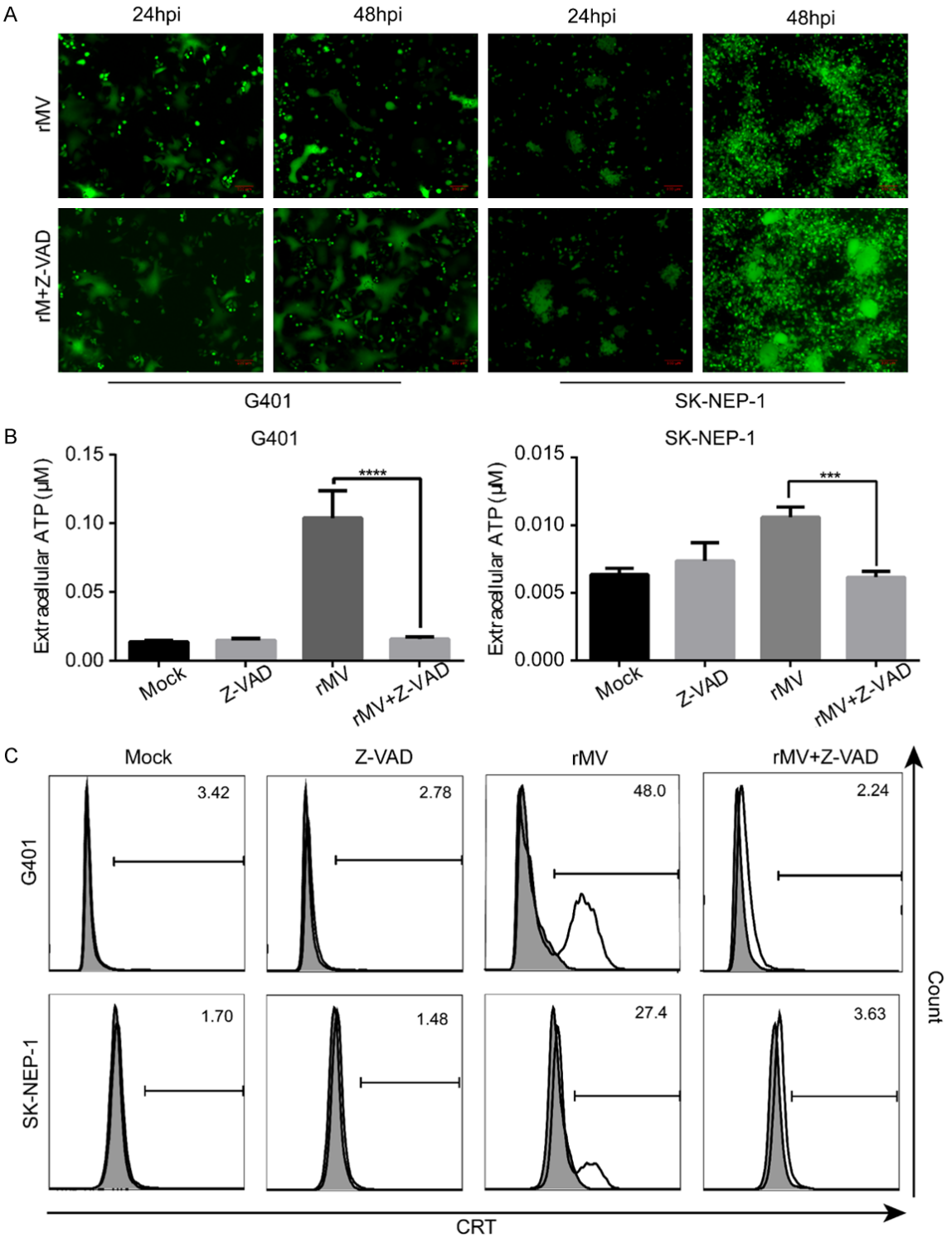

Figure 6. Pharmacological inhibition of apoptosis significantly influenced rMV-Hu191-H-EGFP-induced syncytial death and suppressed DAMPs passive release in MV-infected Nephroblastoma cells. A. G401 and SK-NEP-1 cells infected by rMV-Hu191-H-EGFP at a MOI=0.1 were cultured with Z-VAD. MV-induced syncytia were evaluated on a fluorescence microscope at 24 and 48 hpi. B. G401 and SK-NEP-1 cells were treated with Z-VAD, following infection of rMV-Hu191-H-EGFP at MOI=0.1 for 36 h, and then cell-free supernatants were collected. Decreased ATP level was measured by ATP assay Kit. C. CRT surface expression on nephroblastoma cells in the presence of Z-VAD (50 μM) was determined after 48 hpi of rMV-Hu191-H-EGFP (MOI=0.5). ***=P<0.001; ****=P<0.0001.

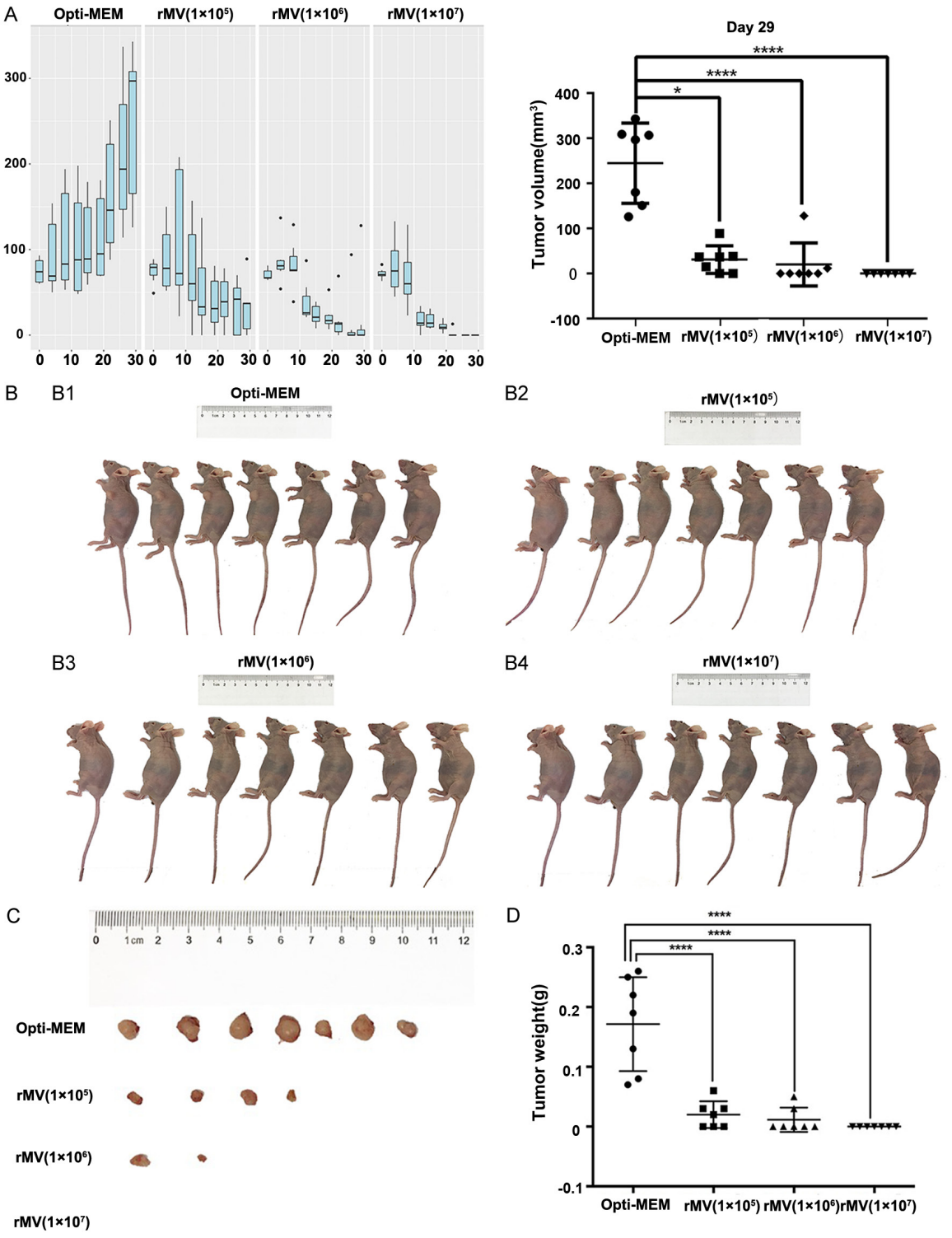

Figure 7. Dose-dependent antitumoral activity of rMV-Hu191-H-EGFP in G401 xenografts after intratumoral injection. A. Nude mice bearing G401 nephroblastoma tumors received intratumoral injections with different doses (1×10^7, 1×10^6 or 1×10^5 PFU in a volume of 100 μl) of rMV-Hu191-H-EGFP or Opti-MEM every other day for 10 days (n=7 each group); tumor size was determined every 4 days. B. Representative photograph of sham-inoculated and rMV-Hu191-H-EGFP-inoculated mice at 29th day post-injection. C. Tumors were collected 29 days after the first injection, and size was compared qualitatively. D. The tumor mass in the sham-inoculated group was significantly greater than in the virus-inoculated groups. ****=P<0.0001.

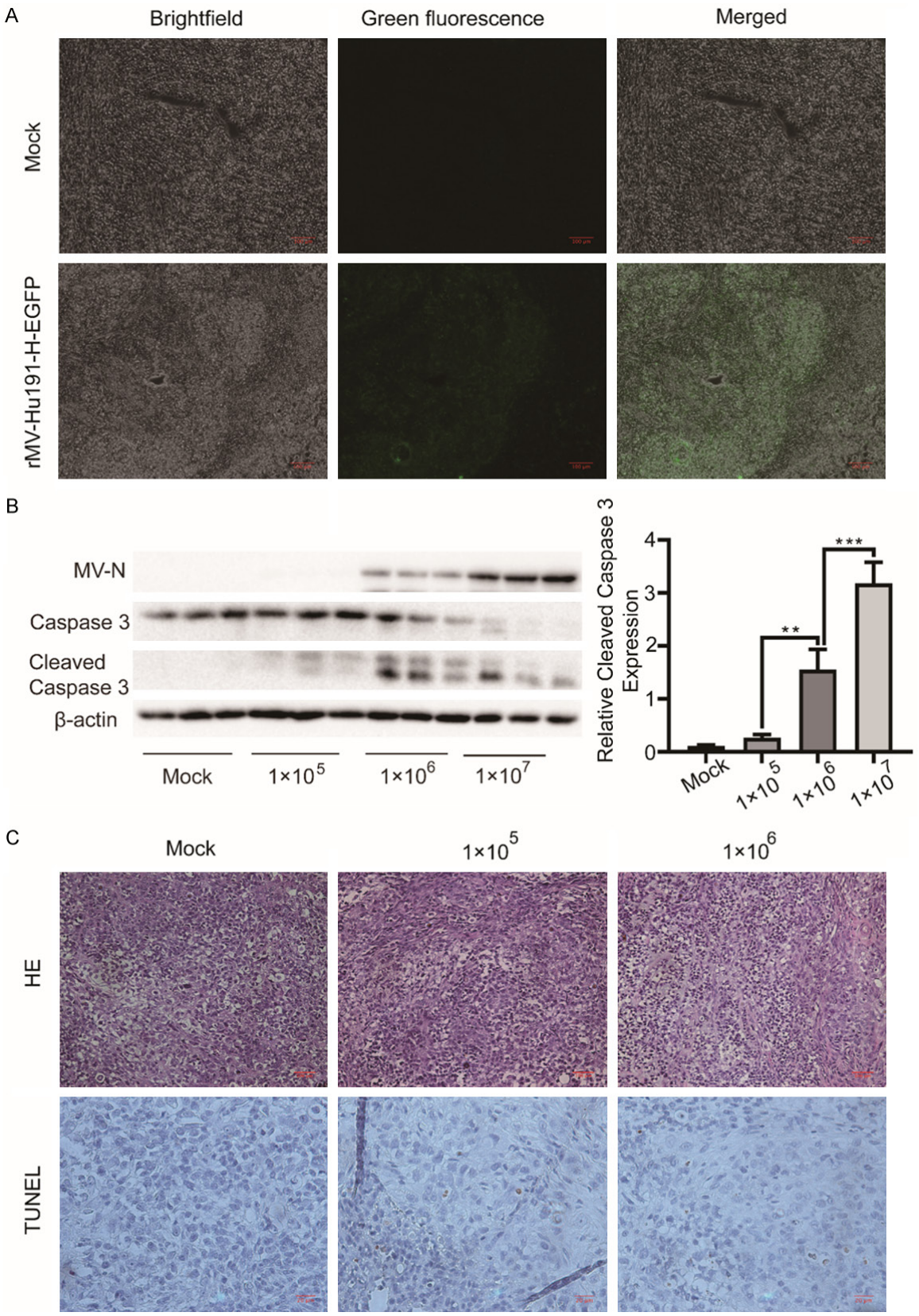

Figure 8. Virus replication and apoptosis were detected in G401 xenograft tumors injected with rMV-Hu191-H-EGFP. A. Mice bearing nephroblastoma xenografts inoculated with 1×10^7 PFU rMV-Hu191-H-EGFP (n=4) or Opti-MEM (n=4) were euthanized at 15 days after the first intratumoral injection. Specific fluorescence was detected in rMV-

Hu191-H-EGFP-infected tumors by fluorescence microscopy. B. Tumor samples were gathered at 15 days after first intratumoral injection, and the MV N protein was detected by Western blot in three tumor samples from each group. Levels of cleaved-caspase-3 were evaluated by Western blot in tumor samples 30 days after the first injection. C. Hematoxylin-eosin (H-E) and TUNEL assay were performed by staining of nephroblastma xenograft tumors 29 days after the first intratumoral virus injection *in vivo* with a dose of 1×10^6 and 1×10^5 PFU. Scale bar =100 μm.

tor CD46 but not nectin-4. The antitumoral effect of rMV-Hu191 was MOI-dependent and resulted in decreased tumor cell proliferation *in vitro*. In our study we observed that rMV-Hu191 also could inhibit the proliferation of HFF-1 cell growth, but a higher MOI was required to achieve a weaker reduction of cell growth (Figure S1). Both unmodified attenuated MV-Edm strain and engineered oncolytic MV-Edm (with no modification with respect to targeting) were reported safe in clinical studies; however, specific viral modifications, such as targeting, shielding and arming, may result in a safer rMV-Hu191 that cannot proliferate in common cells and can possess a stronger oncolytic efficacy.

In the present study we showed for the first time that MV-Hu191 could efficiently express exogenous genes. Three rMVs expressing EGFP at different loci of the MV-Hu191 genome were successfully recovered, suggesting that expression of other foreign genes may be possible by adopting this strategy. Following the novel construction strategy used in this study, MV-Hu191, an authorized vaccine in China, could be efficiently engineered and employed to improve the immunostimulatory capacity of the virus and could be armed with tumor-specific target genes. This will greatly accelerate future research on oncolytic activity of rMV in China.

We illustrated that the rMV-Hu191 with EGFP inserted between the H and L genes exhibited significant antitumor activity and decreased viability of nephroblastoma cells *in vivo*. It was very exciting that mice intratumorally injected with rMV-Hu191-H-EGFP at a dose of 1×10^7 PFU exhibited a superior effect in tumor therapy, with complete elimination of tumors in all the G401 xenograft mice. Even injection with a lower dose of rMV-Hu191-H-EGFP produced excellent antitumor activity. Despite these exciting results in the mouse model and the remarkable safety record of MV-Hu191, suitable models, such as $IFN^{(KO)}$ CD46Ge mice and Rhesus macaques used in toxicology studies, are essential to ensure safety of patients prior to clinical translation of rMV-Hu191 [57, 58].

Previous studies have reported that apoptosis plays an important role in MV-triggered cell death [39, 40]. In the present study we observed that rMVs induced tumor cell death primarily through MV-triggered syncytium formation and apoptosis. Apoptosis was clearly observed during rMV-Hu191-H-EGFP infection, as illustrated by Western blot of caspase-3 and PARP. Interestingly, inhibition of caspase-dependent apoptosis by the broad-spectrum caspase inhibitor Z-VAD did not impact the MV-induced syncytium formation, but syncytial survival was obviously extended in G401 and SK-NEP-1 cells. ICD mediated by DAMPs including CRT, ATP and HMGB1 is a concept that has emerged in recent years [44]. Some OVs including MV have been proven to induce ICD by secretion of ATP and HMGB1 [58-61]. In the present study we also found that MV-induced nephroblastoma cell death was accompanied by passive release of DAMPs (specifically CRT, HMGB1 and ATP) in a MOI-dependent manner, suggesting that rMV-induced cell death may be related to ICD.

In conclusion, we have shown that the attenuated MV vaccine strain MV-Hu191 widely used in China exerts a potent antitumor capacity against nephroblastoma *in vitro* and *in vivo*, demonstrating it to be good candidate for efficient expression of exogenous genes. Furthermore, we illustrated that rMV-Hu191-H-EGFP induced an immunogenic form of apoptosis in nephroblastoma cells that is recognized to result in cross presentation of tumor-associated antigens to dendritic cells (DC) and to other antigen presenting cells, priming antitumor innate and adaptive immunity. Future studies will be aimed at toxicology and antitumor immune response in MV-induced antitumor effects, or even in combination with other immunotherapy strategies, with possible utility in clinical trials.

Acknowledgements

The professional editing service NB Revisions was used for technical preparation of the text prior to submission. This work was supported partly by Science Technology Research Program of Zhejiang Province (2017C33047), Sci-

entific Research Project of Zhejiang Education Department (N20140124); The National Natural Science Foundation for Young Scholars of China (81901679), the Natural Science Foundation for Young Scholars of Zhejiang Province (LQ19H100005) and China Postdoctoral Science Foundation (2019M662076).

Disclosure of conflict of interest

None.

Abbreviations

rMV-Hu191, Recombinant Chinese Hu191 measles virus; OVs, Oncolytic viruses; CPE, cytopathic effect; EGFP, enhanced green fluorescent protein; MOI, multiplicity of infection; ICD, immunogenic cell death; DAMPs, damage-associated molecular pattern; CRT, careticulin; HMGB1, high-mobility group box 1.

Address correspondence to: Zhengyan Zhao, Zhejiang University School of Medicine, Hangzhou, Zhejiang, China; Children's Hospital, Zhejiang University School of Medicine, Hangzhou 310052, Zhejiang, China. Tel: +86-13805722351; Fax: +86-0571-86658672; E-mail: zhaozy@zju.edu.cn

References

[1] Gleason JM, Lorenzo AJ, Bowlin PR and Koyle MA. Innovations in the management of Wilms' tumor. Ther Adv Urol 2014; 6: 165-176.

[2] Njuguna F, Martijn HA, Kuremu RT, Saula P, Kirtika P, Olbara G, Langat S, Martin S, Skiles J, Vik T, Kaspers GJL and Mostert S. Wilms tumor treatment outcomes: perspectives from a low-income setting. J Glob Oncol 2017; 3: 555-562.

[3] Reinhard H, Schmidt A, Furtwangler R, Leuschner I, Rube C, Von Schweinitz D, Zoubek A, Niggli F and Graf N. Outcome of relapses of nephroblastoma in patients registered in the SIOP/GPOH trials and studies. Oncol Rep 2008; 20: 463-467.

[4] Venkatramani R, Malogolowkin MH and Mascarenhas L. Treatment of multiply relapsed wilms tumor with vincristine, irinotecan, temozolomide and bevacizumab. Pediatr Blood Cancer 2014; 61: 756-759.

[5] Weirich A, Ludwig R, Graf N, Abel U, Leuschner I, Vujanic GM, Mehls O, Boos J, Beck J, Royer-Pokora B and Voute PA. Survival in nephroblastoma treated according to the trial and study SIOP-9/GPOH with respect to relapse and morbidity. Ann Oncol 2004; 15: 808-820.

[6] Wegert J, Vokuhl C, Ziegler B, Ernestus K, Leuschner I, Furtwangler R, Graf N and Gessler M. TP53 alterations in Wilms tumour represent progression events with strong intratumour heterogeneity that are closely linked but not limited to anaplasia. J Pathol Clin Res 2017; 3: 234-248.

[7] Godzinski J. The current status of treatment of Wilms' tumor as per the SIOP trials. J Indian Assoc Pediatr Surg 2015; 20: 16-20.

[8] Kaufman HL, Kohlhapp FJ and Zloza A. Oncolytic viruses: a new class of immunotherapy drugs. Nat Rev Drug Discov 2015; 14: 642-662.

[9] Fajardo CA, Guedan S, Rojas LA, Moreno R, Arias-Badia M, de Sostoa J, June CH and Alemany R. Oncolytic adenoviral delivery of an EGFR-targeting T-cell engager improves antitumor efficacy. Cancer Res 2017; 77: 2052-2063.

[10] Zhao D, Chen P, Yang H, Wu Y, Zeng X, Zhao Y, Wen Y, Zhao X, Liu X, Wei Y and Li Y. Live attenuated measles virus vaccine induces apoptosis and promotes tumor regression in lung cancer. Oncol Rep 2013; 29: 199-204.

[11] Chia SL, Yusoff K and Shafee N. Viral persistence in colorectal cancer cells infected by Newcastle disease virus. Virol J 2014; 11: 91.

[12] Gourd E. Oncolytic virus therapy in advanced melanoma. Lancet Oncol 2017; 18: e649.

[13] Jing Y, Chavez V, Ban Y, Acquavella N, El-Ashry D, Pronin A, Chen X and Merchan JR. Molecular effects of stromal-selective targeting by uPAR-retargeted oncolytic virus in breast cancer. Mol Cancer Res 2017; 15: 1410-1420.

[14] Zhang QS, Zhang M, Huang XJ, Liu XJ and Li WP. Apoptosis-inducing effect of myxoma virus on human neuroglioma cell lines. Exp Ther Med 2017; 14: 344-348.

[15] Myers R, Greiner S, Harvey M, Soeffker D, Frenzke M, Abraham K, Shaw A, Rozenblatt S, Federspiel MJ, Russell SJ and Peng KW. Oncolytic activities of approved mumps and measles vaccines for therapy of ovarian cancer. Cancer Gene Ther 2005; 12: 593-599.

[16] Baldo A, Galanis E, Tangy F and Herman P. Biosafety considerations for attenuated measles virus vectors used in virotherapy and vaccination. Hum Vaccin Immunother 2016; 12: 1102-1116.

[17] Msaouel P, Opyrchal M, Domingo Musibay E and Galanis E. Oncolytic measles virus strains as novel anticancer agents. Expert Opin Biol Ther 2013; 13: 483-502.

[18] Russell SJ and Peng KW. Measles virus for cancer therapy. Curr Top Microbiol Immunol 2009; 330: 213-241.

[19] Radecke F, Spielhofer P, Schneider H, Kaelin K, Huber M, Dotsch C, Christiansen G and Billeter MA. Rescue of measles viruses from cloned DNA. EMBO J 1995; 14: 5773-5784.

[20] Peng KW. Systemic therapy of myeloma xenografts by an attenuated measles virus. Blood 2001; 98: 2002-2007.

[21] Dorig RE, Marcil A, Chopra A and Richardson CD. The human CD46 molecule is a receptor

for measles virus (Edmonston strain). Cell 1993; 75: 295-305.
[22] Msaouel P, Dispenzieri A and Galanis E. Clinical testing of engineered oncolytic measles virus strains in the treatment of cancer: an overview. Curr Opin Mol Ther 2009; 11: 43-53.
[23] Muhlebach MD, Mateo M, Sinn PL, Prufer S, Uhlig KM, Leonard VH, Navaratnarajah CK, Frenzke M, Wong XX, Sawatsky B, Ramachandran S, McCray PB Jr, Cichutek K, von Messling V, Lopez M and Cattaneo R. Adherens junction protein nectin-4 is the epithelial receptor for measles virus. Nature 2011; 480: 530-533.
[24] Noyce RS and Richardson CD. Nectin 4 is the epithelial cell receptor for measles virus. Trends Microbiol 2012; 20: 429-439.
[25] Msaouel P, Iankov ID, Allen C, Morris JC, von Messling V, Cattaneo R, Koutsilieris M, Russell SJ and Galanis E. Engineered measles virus as a novel oncolytic therapy against prostate cancer. Prostate 2009; 69: 82-91.
[26] McDonald CJ, Erlichman C, Ingle JN, Rosales GA, Allen C, Greiner SM, Harvey ME, Zollman PJ, Russell SJ and Galanis E. A measles virus vaccine strain derivative as a novel oncolytic agent against breast cancer. Breast Cancer Res Treat 2006; 99: 177-184.
[27] Mateo M, Sinn PL, Navaratnarajah CK, Mendoza C, Donohue R and Cattaneo R. Measles virus rapid and discreet epithelial spread through nectin-4: implications for oncolytic virotherapy. Mol Ther 2014; 22: S10.
[28] Hutzen B, Raffel C and Studebaker AW. Advances in the design and development of oncolytic measles viruses. Oncolytic Virother 2015; 4: 109-118.
[29] Zuniga A, Wang Z, Liniger M, Hangartner L, Caballero M, Pavlovic J, Wild P, Viret JF, Glueck R, Billeter MA and Naim HY. Attenuated measles virus as a vaccine vector. Vaccine 2007; 25: 2974-2983.
[30] Veinalde R, Grossardt C, Hartmann L, Bourgeois-Daigneault MC, Bell JC, Jager D, von Kalle C, Ungerechts G and Engeland CE. Oncolytic measles virus encoding interleukin-12 mediates potent antitumor effects through T cell activation. Oncoimmunology 2017; 6: e1285992.
[31] Li H, Peng KW, Dingli D, Kratzke RA and Russell SJ. Oncolytic measles viruses encoding interferon beta and the thyroidal sodium iodide symporter gene for mesothelioma virotherapy. Cancer Gene Ther 2010; 17: 550-558.
[32] Robinson S and Galanis E. Potential and clinical translation of oncolytic measles viruses. Expert Opin Biol Ther 2017; 17: 353-363.
[33] Zhang Y, Zhou J, Bellini WJ, Xu W and Rota PA. Genetic characterization of Chinese measles vaccines by analysis of complete genomic sequences. J Med Virol 2009; 81: 1477-1483.
[34] Wang Y, Liu R, Lu M, Yang Y, Zhou D, Hao X, Zhou D, Wang B, Li J, Huang YW and Zhao Z. Enhancement of safety and immunogenicity of the Chinese Hu191 measles virus vaccine by alteration of the S-adenosylmethionine (SAM) binding site in the large polymerase protein. Virology 2018; 518: 210-220.
[35] Matveeva OV, Guo ZS, Shabalina SA and Chumakov PM. Oncolysis by paramyxoviruses: multiple mechanisms contribute to therapeutic efficiency. Mol Ther Oncolytics 2015; 2: 10511.
[36] Zhang Y, Wei Y, Zhang X, Cai H, Niewiesk S and Li J. Rational design of human metapneumovirus live attenuated vaccine candidates by inhibiting viral mRNA cap methyltransferase. J Virol 2014; 88: 11411-11429.
[37] Zhou D, Zhu MY, Wang YL, Hao XQ, Zhou DM, Liu RX, Zhang CD, Qu CF and Zhao ZY. Attenuated MuV-S79 as vector stably expressing foreign gene. World J Pediatr 2019; 15: 511-515.
[38] Zhou D, Zhu MY, Wang YL, Hao XQ, Zhou DM, Liu RX, Zhang CD, Qu CF and Zhao ZY. Establishment of an efficient reverse genetic system of Mumps virus S79 from cloned DNA. World J Pediatr 2019; 15: 499-505.
[39] Richetta C, Gregoire IP, Verlhac P, Azocar O, Baguet J, Flacher M, Tangy F, Rabourdin-Combe C and Faure M. Sustained autophagy contributes to measles virus infectivity. PLoS Pathog 2013; 9: e1003599.
[40] Xia M, Meng G, Jiang A, Chen A, Dahlhaus M, Gonzalez P, Beltinger C and Wei J. Mitophagy switches cell death from apoptosis to necrosis in NSCLC cells treated with oncolytic measles virus. Oncotarget 2014; 5: 3907-3918.
[41] Boisgerault N, Guillerme JB, Pouliquen D, Mesel-Lemoine M, Achard C, Combredet C, Fonteneau JF, Tangy F and Gregoire M. Natural oncolytic activity of live-attenuated measles virus against human lung and colorectal adenocarcinomas. Biomed Res Int 2013; 2013: 387362.
[42] Lin EH, Salon C, Brambilla E, Lavillette D, Szecsi J, Cosset FL and Coll JL. Fusogenic membrane glycoproteins induce syncytia formation and death in vitro and in vivo: a potential therapy agent for lung cancer. Cancer Gene Ther 2010; 17: 256-265.
[43] Cao X, Yang M, Wei RC, Zeng Y, Gu JF, Huang WD, Yang DQ, Li HL, Ding M, Wei N, Zhang KJ, Xu B, Liu XR, Qian QJ and Liu XY. Cancer targeting gene-viro-therapy of liver carcinoma by dual-regulated oncolytic adenovirus armed with TRAIL gene. Gene Ther 2011; 18: 765-777.
[44] Krysko DV, Garg AD, Kaczmarek A, Krysko O, Agostinis P and Vandenabeele P. Immunogenic cell death and DAMPs in cancer therapy. Nat Rev Cancer 2012; 12: 860-875.
[45] Kepp O, Senovilla L, Vitale I, Vacchelli E, Adjemian S, Agostinis P, Apetoh L, Aranda F, Barnaba V, Bloy N, Bracci L, Breckpot K, Brough D, Buque A, Castro MG, Cirone M, Colombo MI, Cremer I, Demaria S, Dini L, Eliopoulos AG, Faggioni A, Formenti SC, Fucikova J, Gabriele L,

Gaipl US, Galon J, Garg A, Ghiringhelli F, Giese NA, Guo ZS, Hemminki A, Herrmann M, Hodge JW, Holdenrieder S, Honeychurch J, Hu HM, Huang X, Illidge TM, Kono K, Korbelik M, Krysko DV, Loi S, Lowenstein PR, Lugli E, Ma Y, Madeo F, Manfredi AA, Martins I, Mavilio D, Menger L, Merendino N, Michaud M, Mignot G, Mossman KL, Multhoff G, Oehler R, Palombo F, Panaretakis T, Pol J, Proietti E, Ricci JE, Riganti C, Rovere-Querini P, Rubartelli A, Sistigu A, Smyth MJ, Sonnemann J, Spisek R, Stagg J, Sukkurwala AQ, Tartour E, Thorburn A, Thorne SH, Vandenabeele P, Velotti F, Workenhe ST, Yang H, Zong WX, Zitvogel L, Kroemer G and Galluzzi L. Consensus guidelines for the detection of immunogenic cell death. Oncoimmunology 2014; 3: e955691.

[46] Martins I, Tesniere A, Kepp O, Michaud M, Schlemmer F, Senovilla L, Seror C, Metivier D, Perfettini JL, Zitvogel L and Kroemer G. Chemotherapy induces ATP release from tumor cells. Cell Cycle 2009; 8: 3723-3728.

[47] Russell SJ, Peng KW and Bell JC. Oncolytic virotherapy. Nat Biotechnol 2012; 30: 658-670.

[48] Waters AM, Friedman GK, Ring EK and Beierle EA. Oncolytic virotherapy for pediatric malignancies: future prospects. Oncolytic Virother 2016; 5: 73-80.

[49] Studebaker AW, Hutzen B, Pierson CR, Shaffer TA, Raffel C and Jackson EM. Oncolytic measles virus efficacy in murine xenograft models of atypical teratoid rhabdoid tumors. Neuro Oncol 2015; 17: 1568-1577.

[50] Galanis E, Atherton PJ, Maurer MJ, Knutson KL, Dowdy SC, Cliby WA, Haluska P Jr, Long HJ, Oberg A, Aderca I, Block MS, Bakkum-Gamez J, Federspiel MJ, Russell SJ, Kalli KR, Keeney G, Peng KW and Hartmann LC. Oncolytic measles virus expressing the sodium iodide symporter to treat drug-resistant ovarian cancer. Cancer Res 2015; 75: 22-30.

[51] Markman M, Webster K, Zanotti K, Peterson G, Kulp B and Belinson J. Survival following the documentation of platinum and taxane resistance in ovarian cancer: a single institution experience involving multiple phase 2 clinical trials. Gynecol Oncol 2004; 93: 699-701.

[52] Galanis E, Hartmann LC, Cliby WA, Long HJ, Peethambaram PP, Barrette BA, Kaur JS, Haluska PJ Jr, Aderca I, Zollman PJ, Sloan JA, Keeney G, Atherton PJ, Podratz KC, Dowdy SC, Stanhope CR, Wilson TO, Federspiel MJ, Peng KW and Russell SJ. Phase I trial of intraperitoneal administration of an oncolytic measles virus strain engineered to express carcinoembryonic antigen for recurrent ovarian cancer. Cancer Res 2010; 70: 875-882.

[53] Zhang SC, Cai WS, Zhang Y, Jiang KL, Zhang KR and Wang WL. Engineered measles virus Edmonston strain used as a novel oncolytic viral system against human neuroblastoma through a CD46 and nectin 4-independent pathway. Cancer Lett 2012; 325: 227-237.

[54] Miest TS, Frenzke M and Cattaneo R. Measles virus entry through the signaling lymphocyte activation molecule governs efficacy of mantle cell lymphoma radiovirotherapy. Mol Ther 2013; 21: 2019-2031.

[55] Patel MR, Jacobson BA, Belgum H, Raza A, Sadiq A, Drees J, Wang H, Jay-Dixon J, Etchison R, Federspiel MJ, Russell SJ and Kratzke RA. Measles vaccine strains for virotherapy of non-small-cell lung carcinoma. J Thorac Oncol 2014; 9: 1101-1110.

[56] Nosaki K, Hamada K, Takashima Y, Sagara M, Matsumura Y, Miyamoto S, Hijikata Y, Okazaki T, Nakanishi Y and Tani K. A novel, polymer-coated oncolytic measles virus overcomes immune suppression and induces robust antitumor activity. Mol Ther Oncolytics 2016; 3: 16022.

[57] Lal S, Peng KW, Steele MB, Jenks N, Ma H, Kohanbash G, Phillips JJ and Raffel C. Safety study: intraventricular injection of a modified oncolytic measles virus into measles-immune, hCD46-transgenic, IFNalphaRko mice. Hum Gene Ther Clin Dev 2016; 27: 145-151.

[58] Takasu A, Masui A, Hamada M, Imai T, Iwai S and Yura Y. Immunogenic cell death by oncolytic herpes simplex virus type 1 in squamous cell carcinoma cells. Cancer Gene Ther 2016; 23: 107-113.

[59] Son HA, Zhang L, Cuong BK, Van Tong H, Cuong LD, Hang NT, Nhung HTM, Yamamoto N and Toan NL. Combination of vaccine-strain measles and mumps viruses enhances oncolytic activity against human solid malignancies. Cancer Invest 2018; 36: 106-117.

[60] Donnelly OG, Errington-Mais F, Steele L, Hadac E, Jennings V, Scott K, Peach H, Phillips RM, Bond J, Pandha H, Harrington K, Vile R, Russell S, Selby P and Melcher AA. Measles virus causes immunogenic cell death in human melanoma. Gene Ther 2013; 20: 7-15.

[61] Jiang H, Rivera-Molina Y, Gomez-Manzano C, Clise-Dwyer K, Bover L, Vence LM, Yuan Y, Lang FF, Toniatti C, Hossain MB and Fueyo J. Oncolytic adenovirus and tumor-targeting immune modulatory therapy improve autologous cancer vaccination. Cancer Res 2017; 77: 3894-3907.

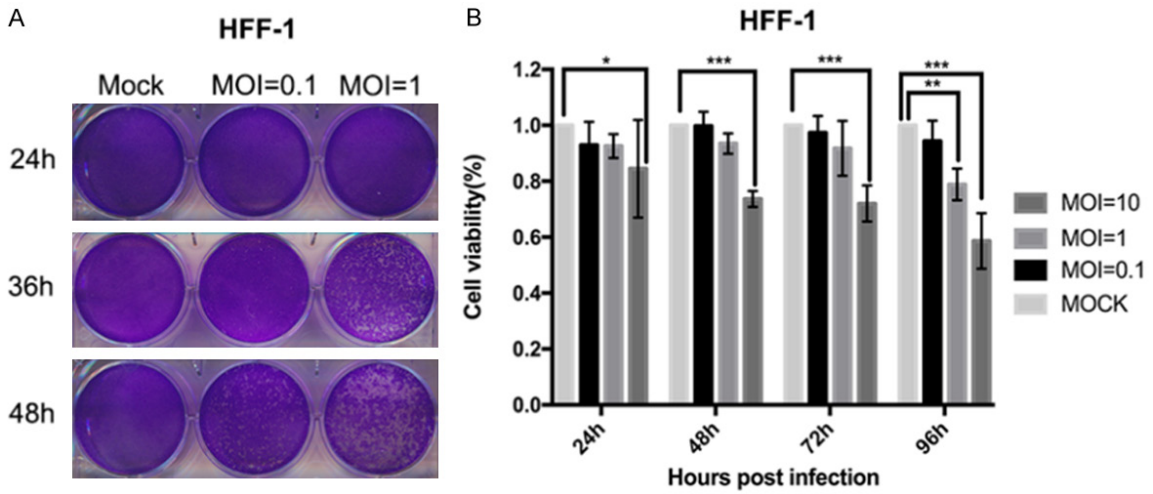

Figure S1. Cytopathic effect, viral growth and killing ability of rMV-Hu191 in HFF-1 cell lines. A. Cytopathic effects were determined in the HFF-1 cell lines by staining with crystal violet every 12 h. B. Confluent HFF-1 cells were infected with rMV-Hu191 at a MOI of 0.1 or 1, and supernatant and cells were collected after three freeze-thaw cycles. Virus titer was testing by plaque assay in Vero cells.